Title

Ultrastructural and SINS analysis of the cell wall integrity response of Aspergillus nidulans to the absence of galactofuranose

Journal

Analyst, 144(3)

ISSN

0003-2654

Authors

Bakir, Görkem

Girouard, Benoit E

Johns, Robert W

et al.

Publication Date

2019-01-28

DOI

10.1039/c8an01591k

Peer reviewed

Journal Name

ARTICLE

Ultrastructural and SINS analysis of the cell wall integrity response of *Aspergillus nidulans* to the absence of galactofuranose

Received 00th January 20xx,
Accepted 00th January 20xx

DOI: 10.1039/x0xx00000x

www.rsc.org/

Gorkem Bakir[a], Benoit Girouard[a], Robert W. Johns[b], Catherine R-J. Findlay[a], Hans A. Bechtel[b], Max Eisele[c], Susan G.W. Kaminskyj[d], Tanya E. S. Dahms[e], Kathleen M. Gough[a]

Abstract With lethal opportunistic fungal infections on the rise, it is imperative to explore new methods to examine virulence mechanisms. The fungal cell wall is crucial for both the virulence and viability of *Aspergillus nidulans*. One wall component, Gal*f*, has been shown to contribute to important fungal processes, integrity of the cell wall and pathogenesis. Here, we explore gene deletion strains lacking the penultimate enzyme in Gal*f* biosynthesis (*ugmAΔ*) and the protein that transports Gal*f* for incorporation into the cell wall (*ugtAΔ*). In applying gene deletion technology to the problem of cell wall integrity, we have employed multiple micro- and nano-scale imaging tools, including confocal fluorescence microscopy, electron microscopy, X-Ray fluorescence and atomic force microscopy. Atomic force microscopy allows quantification of ultrastructural cell wall architecture while near-field infrared spectroscopy provides spatially resolved chemical signatures, both at the nanoscale. Here, for the first time, we demonstrate correlative data collection with these two emerging modalities for the multiplexed *in situ* study of the nanoscale architecture and chemical composition of fungal cell walls.

Introduction

Invasive opportunistic fungal infections are becoming increasingly prevalent in hospital patients, particularly those with cancer who receive immunosuppressive medications, those with HIV who are treated with broad-spectrum antibiotics, and those receiving organ and hematopoietic stem cell transplants, catheters, or prosthetics.[1-3] Invasive aspergillosis, caused by *Aspergillus* spp., arises in a significant portion of such patients, resulting in increased hospital readmissions, duration of stay and mortality.[4]

The virulence and viability of opportunistic fungal pathogens is directly dependent on the biosynthesis, architecture, composition, and integrity of their fungal cell walls, which surround, support, and protect the cell and mediate interactions with the environment. The cell wall integrity (CWI) signalling pathway regulates cell wall biosynthesis as well as the cell division cycle, allowing fungal cells to coordinate responses to a diverse set of adverse conditions.[5,6] Accordingly, these walls and pathways have long been prime targets for the development of antifungal drugs.[7,8]

Like all fungi, *Aspergillus* cell walls are a complex matrix of chitin fibrils, α- and β-glucans, galactomannans, other sugars, proteins and glycoproteins.[2,9] Galactofuranose (Gal*f*), a polysaccharide and glycoconjugate component, is a minor component of the cell wall by weight. Nonetheless, Gal*f* is important for fungal growth, adhesion, morphogenesis, wall architecture, spore development and pathogenesis. It is often found in *Aspergillus* fungal-type galactomannan[9] and glycoproteins (e.g. O-mannose glycans, N-glycans) which modify extracellular enzymes and cell wall proteins.[10-12] UDP-galactopyranose mutase catalyzes the final step in UDP-Gal*f* biosynthesis while the UDP-galactofuranose transporter moves Gal*f* out of the cell for incorporation into the cell wall. Gene deletion strains *ugmAΔ*[13] and *ugtAΔ*[14], which lack the mutase catalyst and transporter enzymes, respectively, were developed to explore the possible role of Gal*f* in CWI. Interestingly, whole cell ELISA quantification and total immunofluorescence intensity of *ugmAΔ* showed higher levels of α-glucan, controlled by CWI pathways, and lower levels of β-glucan compared to wild type.[15] Both gene deletion strains were more susceptible to caspofungin (which inhibits β-glucan synthesis), while the sensitivity to Calcofluor and Congo red (which bind to chitin and various polymeric glucans) was similar to that of wild type.[14-16]

We have imaged fungi and their cell walls in multiple ways, including confocal fluorescence microscopy, scanning and transmission electron microscopy (SEM, TEM),[13-17] atomic force microscopy (AFM), force spectroscopy (FS),[17] and X-Ray fluorescence.[18] We next sought spatially-resolved chemical imaging of the cell wall using vibrational spectra of hyphae, *in situ*. Information obtained from vibrational spectroscopy

[a] *Department of Chemistry, University of Manitoba, R3T 2N2, Winnipeg, Canada*
[b] *Advanced Light Source Division, Lawrence Berkeley National Lab, 94720, Berkeley, USA.*
[c] *Neaspec GmbH, Bunsenstrasse 5, 82512 Martinsried, Germany*
[d] *Department of Biology, University of Saskatchewan, S7N 5E2 Saskatoon, Canada.*
[e] *Department of Chemistry and Biochemistry, University of Regina, S4S 0A2, Regina, Canada.*

† Footnotes relating to the title and/or authors should appear here.
Electronic Supplementary Information (ESI) available: [details of any supplementary information available should be included here]. See DOI: 10.1039/x0xx00000x

(Infrared and Raman) has enabled us to clarify distinctions among species, including differing effects of pH and temperature stress on mature hypha.[19,20] Growing tips and sporulating hyphae have been characterized,[21] along with the identification and spatial location of secondary metabolites.[22,23] Our efforts to obtain vibrational spectroscopic signatures from cell walls have proved challenging, as the wall is typically only tens of nm thick, with a composition that changes along the length behind the growing tip during maturation. Neither whole cell Fourier-transform infrared (FTIR) imaging[19-21] nor surface enhanced Raman spectroscopy[24,25] were successful. To address this problem, we chose a novel correlative approach that would allow us to probe morphology and cell wall ultrastructure via AFM, and explore the spectrochemical composition of the cell wall at nano-scale spatial resolution, *viz*. near-field IR.

Synchrotron infrared nanospectroscopy (SINS) at the Advanced Light Source (ALS) illuminates an AFM tip with synchrotron infrared radiation which is used to probe a target.[26] Thus, SINS enables AFM imaging and near-field broadband infrared spectroscopy with a tip-limited spatial resolution of < 30 nm, to simultaneously examine spatially-resolved envelope ultrastructure and chemical composition at high resolution. This is a proven technique; however, the majority of studies have been on hard, mostly inorganic materials, with only a few focussing on biological targets, and most of the latter are on purified nano-size components.[28-32] The tip-substrate coupling required to obtain scatter is weaker for soft organic materials.[33]

Here we report the first near-field infrared study of chemical differences in the cell walls of wild type *A. nidulans* and the two gene deletion strains, *ugmAΔ* and *ugtAΔ.* Our results illustrate how the combined results of AFM (and potentially AFM-FS) data with the spectrochemical information obtained from near-field infrared spectroscopy can open new avenues for the exploration of cell wall function and composition, *in situ*, at the nanoscale.

Methods

Strains and culture conditions. Preparation of wild type *A. nidulans* (*A1149*) and gene deletion strains *ugmAΔ* and *ugtAΔ* was similar to that previously described.[18,21] Spores from each strain were streaked onto freshly prepared potato dextrose agar (PDA) in Petri dishes, which were sealed and incubated at 37°C for 24-48 hours to yield mature, sporulating colonies. Several μL of ultrapure water was pipetted onto a freshly prepared gold-coated silicon wafer (AuSi, ~1 cm^2) fixed to a glass microscope slide with double-sided tape. A cube of sterile PDA (~3mm) was pressed into a mature colony to pick up spores and then placed, spore side down, onto the water droplet. The slide assembly was sealed in a humid environment and incubated for 24 to 36 hours. Gene deletion strains grew much more slowly and required longer incubation times. Under these conditions, spores germinated and the emerging hyphae grew out beyond any PDA outwash and onto the pristine gold surface. Once there was sufficient growth, slides were snap frozen at -80 °C, and then air-dried for at least 24 hours. The residual PDA block was peeled off, leaving an imprint, with hyphae for imaging at the periphery (ESI Figure 1A). Even dried, the residual PDA block was at least 1 mm thick, and would have impeded SINS analyses.

Fresh samples of *A1149* and *ugmAΔ* were prepared for each of three SINS experiments at ALS; *ugtAΔ* was analysed during the final data collection session. Multiple points on several hyphae were analysed each time. Similar spectra were acquired at Neaspec, Germany, using their Neaspec nano-FTIR spectroscopy system on one sample of each strain, at points very close to those initially examined with SINS at ALS.

AFM imaging. AFM was performed on the correlative instrument prior to SINS. An AuSi wafer with hyphae was taped to a metal chuck (ESI Figure 1B) and placed in the sample chamber; the SINS AFM unit was mounted above. Hyphae were first viewed by bright-field to identify suitable targets. AFM images were collected in tapping mode using high resonant frequency platinum silicide probes (PtSi-NCH, NanoSensors) with a nominal resonant frequency of 330 kHz and nominal spring constant of 42 N/m. The AFM image was collected across the region of interest, providing height, width and ultrastructural data as well as a nm-scale guide for SINS data collection.

SINS spectral collection. The SINS spectra were collected at points of interest identified in each AFM image. SINS scans were co-added for about 15 minutes to ensure good signal to noise ratio (SNR). Although the ALS ring runs in continuous top-up mode, maintaining a current of 500 mA, the background varied over time. The metal-coated tips are very delicate: minute alterations in the tip coating and adherence of particles change the scattering properties. Contamination occurred more often during lengthy AFM topographic scans of the soft protein/carbohydrate hyphal surfaces. Accordingly, a fresh background spectrum was acquired at a clean gold surface after every few spectra, to ensure that sample spectra were consistent with reference signals. Tip quality always degraded over time and tips had to be replaced every day or two.

Neaspec spectral collection. In this system, the AFM tip is illuminated with a laser-based broadband mid-IR nano-FTIR illumination unit to perform nanoscale infrared spectroscopy. The spectra measured at Neaspec, GmbH were recorded within less than 5 min at a spectral resolution of 8.3 cm^{-1}, normalized to a background scan acquired on the gold substrate. All spectral data had a zero-fill factor of 4, so that the final spectra were saved at a nominal spectral resolution of 2.1 cm^{-1}.

Processing to obtain near-field IR spectra. Both near-field methods employ the scattering Scanning Near-field Optical Microscopy (sSNOM) arrangement whereby mid-IR light illuminates an AFM tip operated in tapping mode and the second order back-scattered light is recorded. Using interferometric detection schemes, (nano-FTIR) amplitude, $A(\nu)$, and phase, $\Phi(\nu)$, spectra were obtained with nanometer

spatial resolution from the complex-valued second order scattering coefficient, (σ_2),[26-28] given by equation 1:

$$\boldsymbol{\sigma_2(\nu)} = \mathrm{A_2}(\boldsymbol{\nu})\mathrm{e}^{i[\boldsymbol{\varphi(\nu)}]} \qquad (1)$$

The SINS infrared absorbance spectrum was obtained by taking a ratio of this term against a background signal, collected at a near-by clean surface on the gold-coated wafer, and then extracting the imaginary component according to equation 2:

$$\mathrm{Im}\{\boldsymbol{\sigma_2}(\nu)\} = \frac{\mathrm{A_2(hypha, \nu)}}{\mathrm{A_2(gold, \nu)}} \sin[\varphi(\mathrm{hypha}, \nu) - \varphi(\mathrm{gold}, \nu)] \quad (2)$$

The most recent background spectrum was used in each case. Where two backgrounds (one before and one after) were available, both were evaluated and the better spectrum (good signal to noise, flat baseline) was selected.

Post-processing of Neaspec data was done with neaPLOTTER software (Neaspec GmbH, Germany), which effectively performs the same mathematical procedures as above to yield near-field IR absorbance spectra.

Results and Discussion

Bright-field and TEM images

Representative images clearly show the altered growth habits of the gene deletion strains, (Fig.1 A). Bright field images show the long, unbranched hyphae typical of the fast-growing wild type strain, *A1149*, which grew several hundred microns in 24 hours. In comparison, hyphae from gene deletion strains were, as expected, shorter, thicker and highly branched.[13-17] Liquid spread in a thin pool from the PDA block, appearing yellow in the bright field images of strains. Hyphae were located mainly within the residual PDA traces. Only a few hyphae extended beyond the media, and of these only a few lay against the AuSi surface; the latter were suitable for SINS data collection.

Fig. 1 Images of hyphae, right to left, *A1149*, *ugmAΔ* and *ugtAΔ*, respectively **A**) Bright-field images of strains on AuSi wafers for AFM and SINS data collection, photographs at 50x. **B**) TEM of cell walls (adapted from Refs. 13 and 14). Arrows denote dark outer edge of walls. Scale bars in B = 100 nm.

TEM images (Fig. 1B) have shown that *A1149* walls are ~50 nm thick, whereas those of *ugmAΔ* and *ugtAΔ* are three to four times thicker.[13-17] Edges of the walls (arrows in Fig. 1B) are delineated by electron-dense material. The *ugmAΔ* and *ugtAΔ* cytoplasm appeared to be wild type, but the lack of Gal*f* altered the cell wall and, presumably, its composition. [13, 14] The *ugmAΔ* cell wall appeared to be less well organized than wild type; the dark outer layer that defined the wall edge was broken and uneven. Total lack of dark layering within the wall of the *ugtAΔ* strain indicated significantly altered internal composition. A plausible explanation is that this strain has less protein and more carbohydrate, which does not stain strongly;[15] alternatively, there could be some protein, albeit more thinly dispersed in a less well ordered wall. TEM images provide high spatial resolution information on cross sections, but minimal morphological and chemical analyses.

Reproducibility of near-field IR Data

The goal was to obtain near field infrared spectra of the cell wall, uncontaminated by the cellular contents within, making it critical to acquire reproducible data. The challenge included obtaining many spectra in a limited time frame, while samples were relatively fresh. The spatial resolution afforded by near field IR increased the need for many replicate spectra, which was time consuming given the low SNR, at 8 to 18 minutes per spectrum. A second challenge was the limitation imposed by the spectroscopic probe itself. Here, we report steps taken to ensure quality and reproducibility of data.

AFM and Near-field IR of wild type hyphae and exudate. The best AFM images are typically acquired from fixed hyphae with good turgor, so that the AFM tip probes only the topographical surface,[17] excluding contributions from interior structures, but hyphae for SINS were prepared by freezing unfixed hyphae, reducing information content. Furthermore, high resolution AFM imaging would require longer collection times, during which the tip could be damaged before acquisition of SINS data. For proof of principle, the most important consideration was the reproducibility of the near field IR data itself; thus, most AFM images were acquired as surveys for SINS targets, using the PtSi probes.

AFM images of typical targets for near field IR recorded with the SINS instrument showed that wild type hyphae had retained a cylindrical, tubular form, with a maximum height of 400-500 nm along the centre (Fig. 2A). SINS spectra were acquired from the centre of the mature hyphal wall, some 50-100 µm behind the growing tips, from multiple hyphae (Fig. 2B). Spectra in this and other figures were displayed on common scale, and offset for clarity. Note that total intensities of different spectra depend in part on the strength of the tip-substrate coupling, so that the absolute intensities cannot be quantified. However, relative intensities within spectra depend on amounts of the individual functional groups present in the probed volume.

Fig. 2 AFM image (Tapping amplitude) of an *A1149* hypha and associated SINS spectra. **A**) AFM image recorded with 512 x512 pixel resolution, shows mature cell wall and dried droplets (30 – 150 nm height). **B**) SINS spectra from points along mature walls and at putative exudate points (white circles). Spectra have been offset for clarity.

Though individual spectra were noisy, the profiles were very similar to each other and unlike those from far field FTIR experiments.[19-21] In far-field, the Amide I and II bands around 1650 and 1545 cm^{-1} were much more intense than those of the carbohydrate region (900-1200 cm^{-1}). The latter region always presents as a group of overlapping bands, but the number and relative intensity of bands in the SINS spectra were different, *vide infra*. Since the fungal cell wall is rich in carbohydrates, the increased carbohydrate signal was good evidence that the SINS

method was indeed probing the surface, with an estimated voxel edge of 30-40 nm.

Fungi interact with their surroundings bidirectionally, exuding materials to test for nutrients, and imbibing nutrients. AFM of this wild type hyphae showed what appeared to be minute droplets of dried liquid, which were tentatively ascribed to dried exudate. Spectra recorded at random spots were similar, showing both amide and carbohydrate bands. However, this phenomenon was only observed for one hypha out of three different sample preparations and several hyphae observed in each case. Detailed band assignments were not attempted; we concluded that this was a sample preparation issue, possibly due to cell rupture, which we will investigate in future.

Cell thickness and reproducibility. For this study, multiple hyphae from 6 separate preparations of wild type and *ugmAΔ* were studied over three different ALS synchrotron experiments. The gene deletion strains were thicker than wild type, with maximum heights of > 1 μm. The hyphae of the *ugmAΔ* strain is very slow growing; even after 36 hours of incubation, the hyphae barely extended beyond the vestiges of dried agar (Fig. 1 A). The quick freeze and thaw step for mature hyphae on AuSi caused some hyphae to collapse slightly, creating uneven heights reflecting underlying organelles, as seen for a hyphal branch of *umgAΔ* (Fig. 3A). Even at the thinnest locations, the height was ~400 nm above the AuSi wafer. Spectra acquired at points along hyphae in collapsed regions with little underlying structure (Fig. 3B, C) were very similar. The example spectra shown here were acquired from two different hyphae, on different days, by two different operators at approximately the same regions.

Fig. 3 AFM and SINS spectra of *ugmAΔ* hyphal branch. **A**) AFM topography and selected locations for SINS data, at points ~ 400 nm in height. **B**) SINS spectra from four points, recorded on different days, by 2 different operators, were found to be reliably similar, with proper sample preparation and spectral locations selected as shown above.

Reproducibility on different instruments. To test this further, near field infrared spectra were obtained from the same hyphae at nearly the same locations, with SINS and with a Neaspec instrument, for each of the three strains. Both SINS and Neaspec instruments incorporate the sSNOM approach, the SINS illuminated with synchrotron light and the Neaspec with the broadband mid-infrared nano-FTIR illumination unit. The similarity between the spectra is sufficient to give confidence in the main features in all spectral profiles (Fig. 4).

SINS spectra reveal effects of Gal*f* deletion in cell walls

SINS spectra were collected over multiple experiments at ALS. Spectra representative of the three fungal strains, shown in Fig. 4, can now be used for a more detailed spectrochemical analysis. Given that spectra from similar points had similar profiles, individual spectra from comparable locations were summed to improve SNR for all three strains. The only difference introduced by gene deletions was the absence of Galf[13-17] and, as a minor component, its absence should not have a noticeable impact on the wall spectra. Nonetheless, there were significant spectral differences that could aid in our understanding of the downstream impact of the gene deletions.

Fig. 4. Near-field infrared spectra of mature hyphal walls from *wild type*, *ugmAΔ* and *ugtAΔ* strains. SINS spectra are sums of 7-10 spectra, acquired from similar regions, different preparations and dates, and summed for improved SNR. Spectra from Neaspec were acquired from one of each of the three strains at approximately the same locations as probed with SINS at ALS.

In an AFM-FS study of surface architecture, the *ugmAΔ* strain was previously found to be less rough (subunit size ~3x greater than in wild type), and less well ordered, with an elastic modulus one tenth that of normal wild type hyphae. [17] This fact, and the loss of viscoelasticity, indicated that, despite being a minor wall component, Gal*f* likely has a role in cross-linking.

The first obvious difference between the spectra of *wild type* and *ugmAΔ* and *ugtAΔ* gene deletion strains is in the relative intensities of the amide (I & II) and carbohydrate bands (Table 1). The amide bands are the most prominent in the wild type spectra, and much weaker in those of the *ugmAΔ* and *ugtAΔ*. The TEM images showed that the cell walls of the gene deletion strains are 3 to 5 times thicker than the wild type (Fig. 1); decreased staining had been interpreted as a decrease in protein content of the cell walls, with *ugtAΔ* having the least. Reduction of protein content in these strains could explain the reduction in the amide band intensities; however, the N-acetyl groups in chitin also absorb in this region, with band maxima reported to be ~1640 and 1540 cm^{-1} (Table 1). In fungal cell walls, chitin is located at the base of the wall, adjacent to the lipid membrane of the encapsulated cells.[1-3] The thin wall of wild type hyphae (estimated to be 25 – 50 nm) could potentially allow chitin acetamide bands to appear in the SINS spectra but most likely at longer wavelengths than protein. The amide I band maximum in *A1149* is observed at 1655 cm^{-1}, best assigned as α-helical protein rather than chitin. In contrast, the increased wall thickness would preclude detection of the underlying chitin layer in *ugmAΔ* and *ugtAΔ*. The significant loss of intensity at this region in spectra of the gene deletion strains is therefore attributed to lack of protein within cell wall itself. This spectrochemical result is consistent with the physical structure, and further confirms that the SINS spectra are probing the surface of the hyphae.

Overall, spectra of both gene deletion strains exhibit much higher relative intensity than *wild type* in the 1150 to 900 cm^{-1} region, variously attributed to carboxymethyl groups of glucans.[34-37] Amide and chitin bands are well known; however, literature assignments for glucan bands are hampered by problems with sample consistency. Literature values reported for these compounds are often based on partially refined extracts from various natural sources, ranging from shellfish and insects to fungi and yeasts. Our analyses of the spectra in the 1150-900 cm^{-1} region are based on peak assignments from spectra of chitin and α- and β-glucans, purified from *A. niger*,[34] *S. cerevisiae*,[34, 35, 37] a moth (*Ephestia kuehniella* Zeller) and commercial shrimp chitin.[36] The *ugmAΔ* and *ugtAΔ* strains have significantly lower peaks than wild type at 1079 cm^{-1} and

significantly higher peaks than wild type at 1130-1155 cm^{-1}. These absorbance bands are assigned to β-glucan and α-glucan, respectively (Table 1). Thus the SINS spectra provide direct evidence that gene deletions preventing Gal*f* from contributing to wall structure induce a response that preferentially increases the α-glucan content.

One of the major advantages of opportunistic fungi is their ability to respond dynamically to threats through pathway regulation.[1-3] Cell wall stresses are known to activate genes responsible for the synthesis of cell wall components such as chitin or α-(1,3) glucan.[38-42] Gal*f* is only a minor component in cell wall, but possible roles for Gal*f* in cell wall synthesis have been noted by us and others.[13-17, 43-46] Based on the cell wall remodelling in strains deficient in Gal*f*, we originally hypothesized that its absence would alter not only the organization of cell wall components, but also their biochemical composition through CWI and other signalling pathways.[13-17]

The typical CWI response is to upregulate certain cell wall components in a compensatory fashion.[2] AFM and TEM of these strains had shown that an absence of Gal*f* significantly altered the cell wall architecture, composition, function and integrity. Nonetheless, this CWI response failed to protect it against certain antifungal drugs,[14-16] underscoring the importance of Gal*f* in cell wall maturation and hyphal extension. The SINS spectra show increases in the α-glucan wall content in the *ugmAΔ* and *ugtAΔ* gene deletion strains, consistent with our previous studies[15] and an *Aspergillus* CWI response.[2]

Conclusions

Next-wave single cell analyses must include the production of highly resolved structural and compositional analyses of biological specimens. For dried samples, AFM reports on gross morphology, nanoscale surface architecture and roughness that can be further articulated by near-field FTIR surface chemical analysis. Here, we have demonstrated how SINS offers powerful multiplexed data with nm-scale resolution that complements and clarifies changes in fungal cell wall integrity induced by genetic alteration. These methods, used in conjunction with existing tools, offer an exciting new way to study previously inaccessible regions of single cells.

Conflicts of interest

There are no conflicts to declare.

Acknowledgements

KMG, SGWK, and TESD acknowledge funding from the Natural Sciences and Engineering Research Council (NSERC) of Canada. GB and CF were supported by the award of a Graduate Enhancement of Tri-Council Stipend (GETS) from the Faculty of graduate Studies, University of Manitoba. CF received a graduate fellowship from Research Manitoba. This research used resources of the Advanced Light Source, which is a DOE Office of Science User Facility under contract no. DE-AC02-05CH11231.

References

1 B. B. Fuchs, E. Mylonakis, *Eukaryot. Cell*, 2009, **8**, 1616-1625.
2 V. Valiante, J. Macheleidt, M. Föge, A. A. Brakhage, *Front, Microbiol.*, 2015, **6**, 325.
3 A. Yoshimi, K. Miyazawa, K. Abe, *Biosci. Biotech. Biochem.*, 2016, **80**, 1700-1711.
4 M. D. Zilberberg, B. H. Nathanson, R. Harrington, J. R. Spalding, A. F. Shorr, *Clin. Infect. Dis.*, 2018, ciy181, https://doi.org/10.1093/cid/ciy181.
5 J. P. Latge, *Mol. Microbiol*., 2007, **66,** 279-290.
6 M. J. Dagley, I. E. Gentle, T. H. Beilharz, F. A. Pettolino, J. T. Djordjevic, T. L. Lo, N. Uwamahoro, T. Rupasinghe, D. L. Tull, M. McConville, et al., *Mol. Microbiol*. 2011, **79**, 968-989.
7 J. R. Perfect, *Med. Mycol. Suppl.*, 2005, **43**, 271-276.
8 P. W. J. De Groot, B. W. Brandt, H. Horiuchi, A. F. J. Ram, C. G. De Koster, F. M. Klis, *Fungal Genet. Biol.*, 2009, **46**, 72-81.
9 J. P. Latgé, H. Kobayashi, J. P. Debeaupuis, M. Diaquin, J. Sarfati, J. M. Wieruszeski, E. Parra, J. P. Bouchara, B. Fournet, 1994, *Infect. Immunol.,* 1994, 5424-5433.
10 G. L.F. Wallis, F. W. Hemming, J. F. Peberdy, *FEMS Microbiol. Lett.,* 2001, **201**, 21-27.
11 M. Goto, *Biosci. Biotech. Biochem.*, 2007, **71**, 1415-1427.
12 B. Tefsen, A. Ram, I. Van Die, F. H. Routier, *Glycobiol.*, 2012, **22**, 456-469.
13 A. M. El-Ganiny, D. A.R. Sanders, S. G.W. Kaminskyj, *Fungal Genet. Biol.*, 2008, **45**, 1533-1542.
14 S. Afroz, A. M. El-Ganiny, D. A. R. Sanders, S. G. W. Kaminskyj, *Fungal Genet. Biol.*, 2011, **48**, 896-903.
15 K. Alam, K. Van Straaten, D. Sanders, S. Kaminskyj, *PLoS ONE*, 2014, **9**, E85735
16 M. K. Alam, A. M. El-Ganiny, S. Afroz, D. A.R. Sanders, J. Liu, S. G.W. Kaminskyj, *Fungal Genet. Biol.*, 2012, **49**, 1033-1043.
17 B. C. Paul, A. M. El-Ganiny, M. Abbas, S. G. W. Kaminskyj, T. E. S. Dahms, *Eukaryot. Cell*, 2011, **10**, 646-653.
18 M. Rak, M. Salome, S. G. W. Kaminskyj, K. M. Gough, *Analyt. Bioanalyt. Chem.,* 2014, **406**, 2809-2816.
19 A. Szeghalmi, S. Kaminskyj, K. M. Gough, *Analyt. Bioanalyt. Chem.*, 2007, **387**, 1779-1789.
20 S. Kaminskyj, K. Jilkine, A. Szeghalmi, K. Gough, *FEMS Microbiol. Lett.,* 2008, **204,** 1-8.
21 K. Jilkine, K. M. Gough, R. Julian, S. G.W. Kaminskyj, *J. Inorg. Biochem.,* 2008, **102**, 540-546.
22 M. Isenor, S. G.W. Kaminskyj, R. J. Rodriguez, R. S. Redman, K. M. Gough, *Analyst*, 2010, **135**, 3249-3254.
23 C. Liao, M. D. Piercey-Normore, J. L. Sorensen, K. Gough, *Analyst*, 2010, **135**, 3242-3248.
24 A. Szeghalmi, S. Kaminskyj, P. Rosch, J. Popp, K. M. Gough, *J. Phys. Chem. B,* 2007, **111**, 12916-12924.
25 M. A. Prusinkiewicz, F. Farazkhorasani, J. J. Dynes, J. Wang, K. M. Gough, S. G.W. Kaminskyj, *Analyst*, 2012, **137**, 4934-4942.
26 H. A. Bechtel, E. A. Muller, R. L. Olmon, M. C. Martina, and M. B. Raschke, *Proc. Natl. Acad. Sci. USA*, 2014, **111**, 7191-7196.
27 S. Mastel, A. A. Govyadinov, T. V. A. G. de Oliveira, I. Amenabar, R. Hillenbrand, *Appl. Phys. Lett.,* 2015, **106**, 023113.
28 R. Wiens, C. R. Findlay, S. G. Baldwin, L. Kreplak, J. M. Lee, S. P. Veres and K. M. Gough, *Farad. Discuss*., 2016, **187**, 555-573.
29 I. Amenabar, S. Poly, W. Nuansing, E. H. Hubrich, A. A. Govyadinov, F. Huth, R. Krutokhvostov, L. Zhang, M. Knez, J. Heberle, A. M. Bittner, and R. Hillenbrand, *Nat. Commun*., 2013, **4**, 1-9.

30 E. A. Muller, B. Pollard, M. B. Raschke, *J. Phys. Chem. Lett*., 2015, **6**, 1275 − 1284
31 N. Qin, S. Zhang, J. Jiang, S. Corder, Z. Qian, Z. Zhou, W. Lee, K. Liu, X. Wang, X. Li, Z. Shi, Y. Mao, H.A. Bechtel, M.C. Martin, et al., *Nat. Comm*., 2016, **7**, 13079.
32 S. Berweger, D. M. Nguyen, E. A. Muller, H. A. Bechtel, M. B. Raschke, *J. Am. Chem. Soc*., 2013, **135**, 18292−18295
33 F. Keilmann, R. Hillenbrand, *Phil. Trans. R. Soc. Lond. A*, 2004, **362**, 787–805
34 J. Šandula, G. Kogan, M. Kačuráková, E. Machová, *Carbohyd. Poly.,* 1999, **38,** 247-253
35 Z. Hromadkova, A. Ebringerova, V. Sasinkova, J. Sandula, V. Hribalova, J. Omelkova, *Carbohyd. Poly.,* 2003, **51**, 9-15.
36 M. Mehranian, R. F. Pourabad, N. S. Bashir, S. Taieban, *J. Macromol. Sci., A*, 2017, **54**, 720-726.
37 V. Zechner-Krpan, V. Petravic-Tominac, I. Gospodaric, L. Sajli, S. Dakovic, J. Filipovic-Grcic, *Food Technol. Biotech.*, 2010, **48,** 189-197.
38 R. A. Damveld, P. A. VanKuyk, M. Arentshorst, F. M. Klis, C. A. M. J. J. van den Hondel, A. F. J. Ram, *Fungal Gen. Biol*., 2005, **42**, 165-177.
39 T. Fujioka, O. Mizutani, K. Furukawa, N. Sato, A. Yoshimi, Y. Yamagata, T. Nakajima, K. Abe, *Eukaryot. Cell*, 2007, **6**, 1497-1510.
40 T. Katayama, A. Ohta, H. Horiuchi, *Biosci. Biotech. Biochem.*, 2015, **79**, 321-330.
41 H. Park, M. Hulsman, M. Arentshorst, M. Breeman, E. Alazi, E. L. Lagendijk, M. C. Rocha, I. Malavazi, B. M. Nitsche, C. A. M. J. J. van den Hondel, *et. al*., *Cell. Microbiol.*, 2016, **18**, 1268-1284.
42 T. Oka, *Biosci. Biotech. Biochem.*, 2018, **82**, 183-191.
43 L. L. Pedersen, S. J. Turco, *Cell. Mol. Life Sci.* 2003, **60**, 259-266.
44 R. A. Damveld, A. Franken, M. Arentshorst, P. J. Punt, F. M. Klis, C. A. M. J. J. van den Hondel, A. F. J. Ram, *Genetics*, 2008, **178**, 873-881.
45 P. S. Schmalhorst, S. Krappmann, W. Vervecken, M. Rohde, M. Müller, G. H. Braus, R. Contreras, A. Braun, H. Bakker, F. H. Routier, *Eukaryot. Cell*, 2008, **7**, 1268-1277.
46 J. Latge, *Med. Mycol*. 2009, **47**, S104-S109.

Table 1. NFIR Band positions (cm^{-1}) and assignments in NFIR of *A. nidulans* strains

A1149	ugmAΔ	ugtAΔ	Assignment
1049	1020-1040	1020-1040	α, β-glucan[a,b]
1079			ν(CO), β-glucan[a]
1116-1130		1113-1125	ν (CC), C-O-C chitin, β-glucan[a,c]
1157	1153	1157	ν (COC), ν (CC) α-glucan[a]
1546	1549	1550	Amide II, β-glucan [b,d]
	1630	1623	ν (C=O) chitin (acetamide) [a,b,d]
1655	1650	1650	Amide I [a,b.d]

[a] Ref. 33 [b] Ref. 34 [c] Ref. 35 [d] Ref. 36

Table of Contents Graphical entry

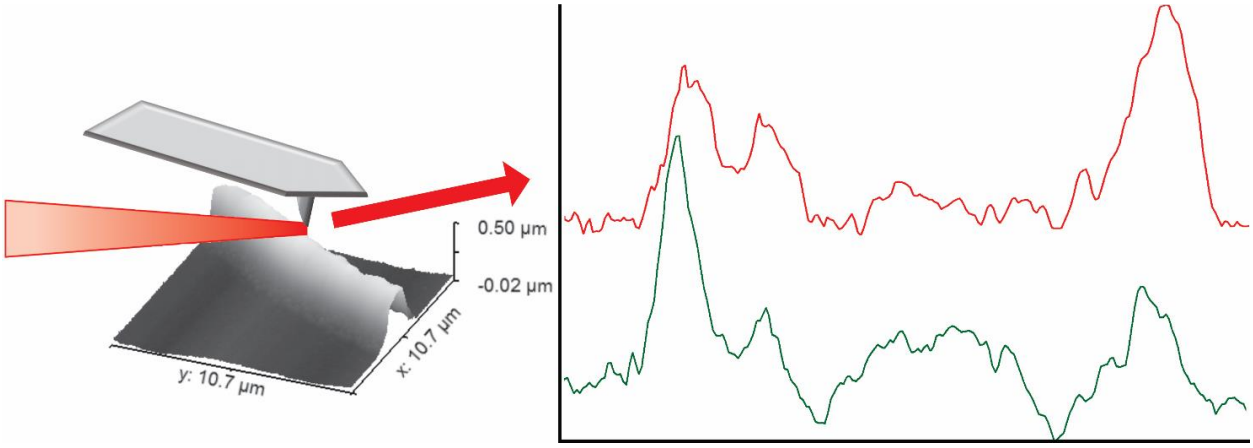

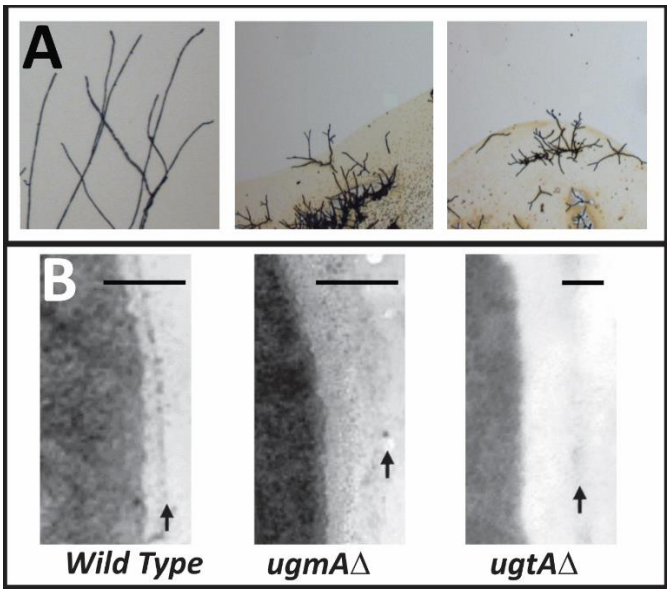

Fig. 1 Images of hyphae, right to left, *A1149*, *ugmAΔ* and *ugtAΔ*, respectively **A**) Bright-field images of strains on AuSi wafers for AFM and SINS data collection, photographs at 50x. **B**) TEM of cell walls (adapted from Refs. 13 & 14). Arrows denote dark outer edge of walls. Scale bars in B = 100 nm.

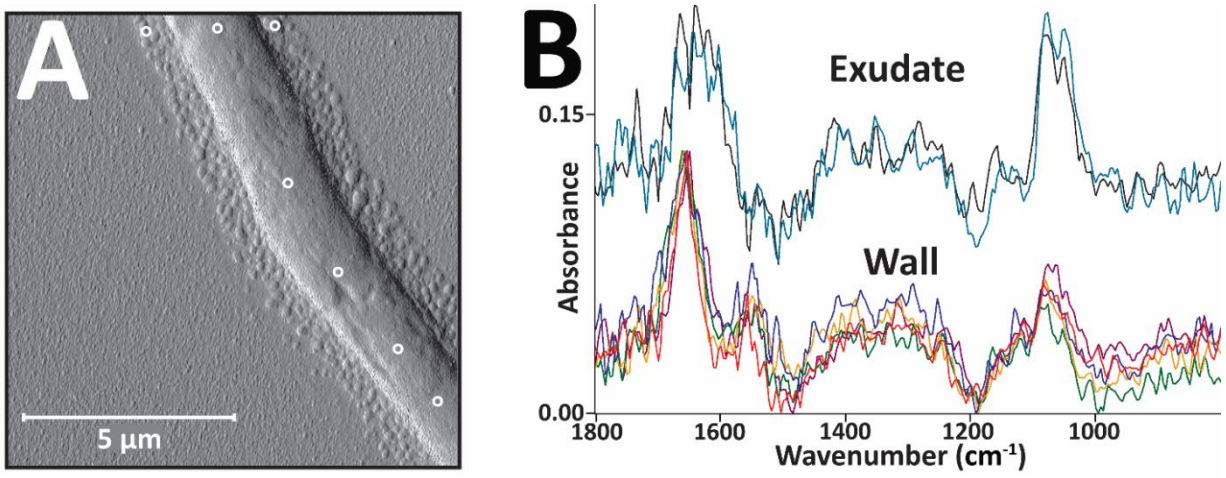

Fig. 2 AFM image (Tapping amplitude) of an *A1149* hypha and associated SINS spectra. **A**) AFM image recorded with 512 x512 pixel resolution, shows mature cell wall and dried droplets (30 – 150 nm height). **B**) SINS spectra from points along mature walls and at putative exudate points (white circles). Spectra have been offset for clarity.

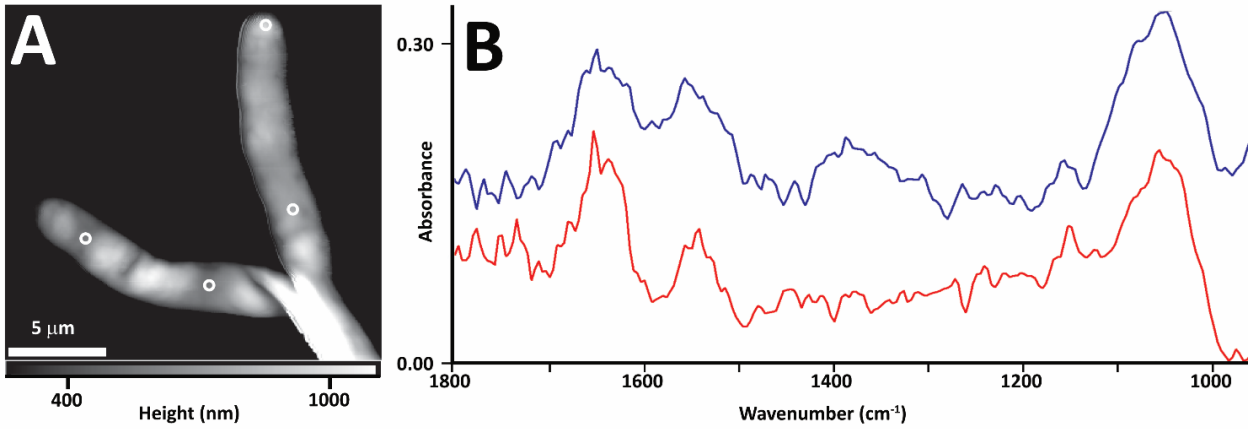

Fig. 3 AFM and SINS spectra of *ugmA⊿* hyphal branch. **A**) AFM topography and selected locations for SINS data, at points ~ 400 nm in height. **B**) SINS spectra from four points, recorded on different days, by 2 different operators, were found to be reliably similar, with proper sample preparation and spectral locations selected as shown above.

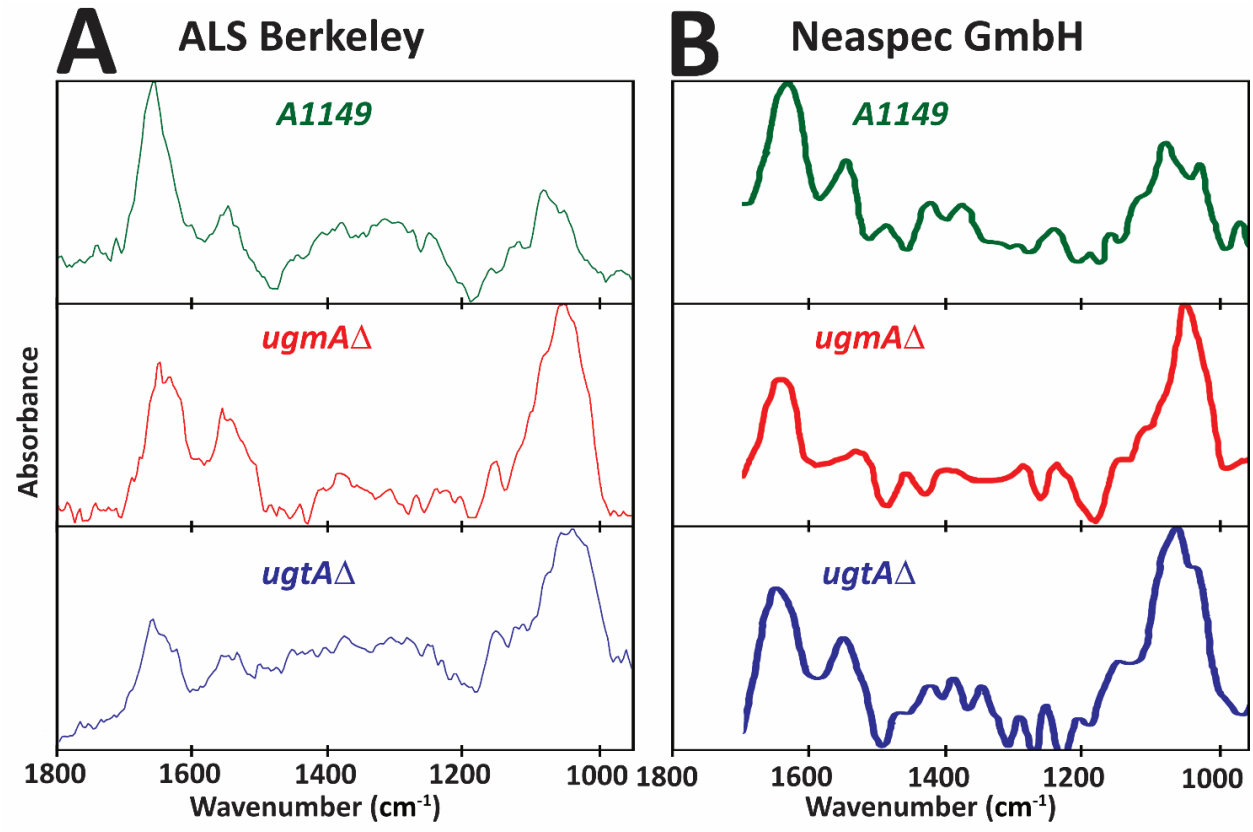

Fig. 4. Near-field infrared spectra of mature hyphal walls from *wild type*, *ugmAΔ* and *ugtAΔ* strains. SINS spectra are sums of 7-10 spectra, acquired from similar regions, different preparations and dates, and summed for improved SNR. Spectra from Neaspec were acquired from one of each of the three strains at approximately the same locations as probed with SINS at ALS.

Electronic Supplementary Information Figure 1.

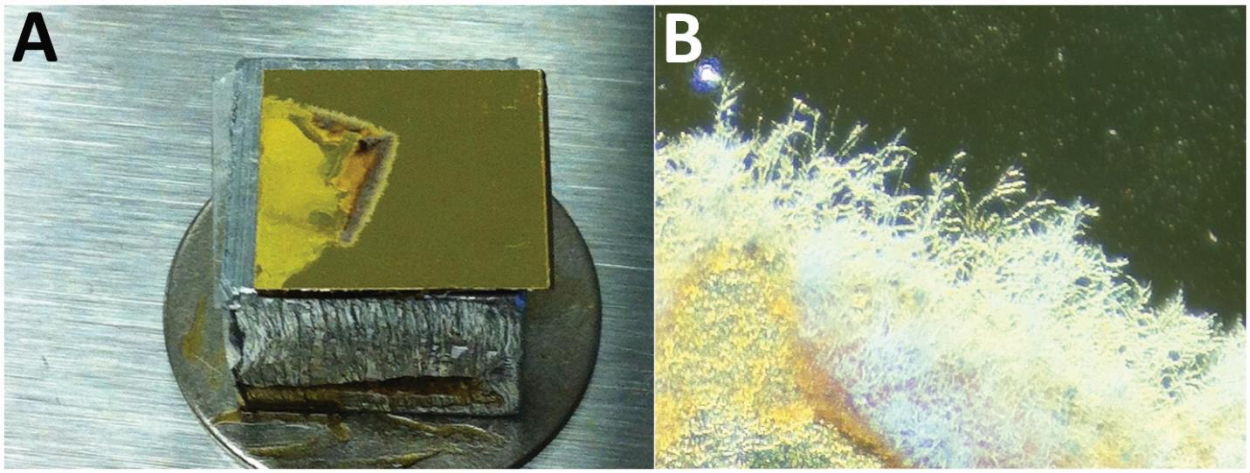

ESI Fig. 1. Sample preparation for SINS experiment. **A.** Gold-coated silicon wafer (~1 cm^2) with dried fungal hyphae preparation (*ugmA*Δ) is taped to metal chuck for mounting in the AFM-SINS sample chamber. The hyphae grew out across the pristine gold surface, from the 3 mm PDA block. The dried PDA block was removed, but the outline remains. Hyphae at the centre are the best positioned for data acquisition. **B.** Photo of the hyphae emerging from the PDA region. More detailed images are given in the manuscript.